



HAL
open science

Large-scale remapping of visual cortex is absent in adult humans with macular degeneration

Heidi Ann Baseler, Andre Gouws, Koen V Haak, Christopher Racey, Michael Crossland, Adnan Tufail, Gary Stuart Rubin, Frans W Cornelissen, Antony Bryan Morland

► To cite this version:

Heidi Ann Baseler, Andre Gouws, Koen V Haak, Christopher Racey, Michael Crossland, et al.. Large-scale remapping of visual cortex is absent in adult humans with macular degeneration. *Nature Neuroscience*, 2011, 10.1038/nn.2793 . hal-00626735

HAL Id: hal-00626735

<https://hal.science/hal-00626735>

Submitted on 27 Sep 2011

HAL is a multi-disciplinary open access archive for the deposit and dissemination of scientific research documents, whether they are published or not. The documents may come from teaching and research institutions in France or abroad, or from public or private research centers.

L'archive ouverte pluridisciplinaire **HAL**, est destinée au dépôt et à la diffusion de documents scientifiques de niveau recherche, publiés ou non, émanant des établissements d'enseignement et de recherche français ou étrangers, des laboratoires publics ou privés.

Large-scale remapping of visual cortex is absent in adult humans with macular degeneration

¹Heidi A Baseler, ¹André Gouws, ²Koen V Haak, ¹Christopher Racey, ^{3,4}Michael D Crossland, ^{3,4}Adnan Tufail, ³Gary S Rubin, ²Frans W Cornelissen and ^{1,5}Antony B Morland.

¹York Neuroimaging Centre, Department of Psychology, University of York, York, YO10 5DD, UK

²Laboratory for Experimental Ophthalmology and BCN Neuroimaging Centre, University Medical Centre Groningen, University of Groningen, Groningen, Netherlands

³Institute of Ophthalmology, University College London, Bath Street, London, UK

⁴Moorfields Eye Hospital NHS Foundation Trust, London, UK

⁵Hull-York Medical School, York, UK

Correspondence should be addressed to ABM (a.morland@psychology.york.ac.uk)

AUTHORSHIP STATEMENT: HAB and AG acquired and analyzed the neuroimaging data and prepared the manuscript; KVH designed and implemented an analysis to determine the population receptive field characteristics and prepared the manuscript; CR acquired neuroimaging data; MDC recruited patients, acquired and analyzed clinical data; AT recruited and assessed patients; GSR jointly designed the study, recruited patients and acquired and analyzed clinical data; FWC designed an analysis to determine the population receptive field characteristics and prepared the manuscript; ABM jointly designed the study, acquired and analyzed the neuroimaging data and prepared the manuscript. All authors have contributed to drafts of the manuscript. AG and KVH have contributed equally and are therefore joint second authors.

ABSTRACT

The occipital lobe contains a retinotopic representation of the visual field. The representation of the central retina in early visual areas (V1-3) is found at the occipital pole. When the central retina is lesioned in both eyes by macular degeneration, this region of visual cortex at the occipital pole is accordingly deprived of input. However, even when such lesions occur in adulthood, some visually driven activity in and around the occipital pole can be observed. It has been suggested that this activity is due to remapping of this area, so that it now responds to inputs from intact, peripheral retina. We evaluated whether or not remapping of visual cortex underlies this activity. Our fMRI results provide no evidence of remapping, questioning the contemporary view that early visual areas of the adult human brain have the capacity to reorganize extensively.

INTRODUCTION

The human brain contains maps of the retina on the surface of the occipital lobes¹. Abnormal visual development can modify these retinotopic maps²⁻⁵. Under circumstances where individuals acquire early visual experience in the presence of a lesion to the center of the retina, reorganization of the visual representation occurs⁶. The visual brain in these individuals remaps by allocating a larger than normal area of cortex to intact, peripheral vision. Although brain plasticity is clearly possible when neural changes occur early in life, the adult brain also appears capable of plasticity. Experimentally-induced retinal lesions in adult animals can lead to a remapping of primary visual cortex to respond to inputs from nearby intact retina⁷⁻¹³. We undertook the present study to determine whether cortical remapping generalizes to humans who acquire retinal lesions in adulthood.

Several groups have investigated reorganization in human adult cortex when retinal lesions were acquired as a result of disease (macular degeneration). These studies have produced variable results, generating some controversy. Sunness et al¹⁴ found no evidence of activity in parts of visual cortex that normally receive input from lesioned retina (the “lesion projection zone”) in a single, elderly patient. Baker and colleagues¹⁵, on the other hand, reported widespread activation of the lesion projection zone in two adult patients with juvenile macular degeneration, and suggested that it might reflect a cortical remapping via horizontal connections similar to, but larger than, those found in earlier animal studies. The remapping hypothesis is supported by another fMRI study claiming that activation of deprived cortex can be generated by eccentric fixation¹⁶. Stimulating the occipital cortex of a patient blinded in adulthood by trauma to the optic nerves resulted in abnormal phosphene maps, also suggesting cortical remapping¹⁷. Despite these reports, the implication that remapping is responsible for the large-scale spread of activation within the lesion projection zone of patients with retinal lesions acquired in adulthood has been seriously questioned¹⁸⁻²⁰.

Using methods that explicitly evaluate visual cortical maps, we sought to determine whether humans with lesions acquired in adulthood exhibit reorganization in the form of cortical remapping of visual input over the large-scale seen in patients with congenital foveal loss of vision⁶. In contrast to prior studies largely restricted to a few patients with juvenile forms of macular degeneration (JMD), we compared responses in a large number of individuals in two different age groups: those with JMD and those with the more common age-related form (AMD), and their age-matched controls. We found no evidence of large-scale remapping in early visual areas in adults with acquired retinal lesions. Indeed, the area of activity in primary visual cortex measured in patients was no different from that predicted on the basis of normal retinotopic maps. Furthermore, the absence of cortical remapping was not dependent on the age at which patients acquired retinal lesions in adulthood.

RESULTS

Cortical responses were measured in 16 patients with macular degeneration (see Table 1) and 12 age-matched controls with normal vision using functional magnetic resonance imaging (fMRI). Patients had bilateral lesions for at least one year and had developed a stable preferred retinal locus that allows good fixation performance. Two age groups were tested, young (mean age 30) and elderly (mean age 76). Participants passively viewed flickering checkerboard stimuli configured in a ring that expanded through

increasing eccentricity or a wedge that rotated around a central point. Such stimuli reliably modulate blood oxygenation level dependent signals and are used to map visual areas in occipital cortex^{1,21-24}. Response magnitude was first evaluated using coherence as an outcome measure, as in previous similar fMRI studies^{18,25} (see Methods).

Figure 1 shows coherence maps in four individuals, one from each of the two patient and control groups. Responses exceeding a coherence of 0.30 are shown superimposed on a smoothed, inflated rendering of the cortical surface of the left occipital lobe in each individual. While control subjects show significant visually driven responses throughout visual cortex, both the young and elderly patients only display significant responses in the anterior occipital lobe. Strong responses in the patients are therefore limited to regions of the cortex that normally map peripheral (i.e. intact) retina (see retinal sensitivity map insets in Figure 1, derived from microperimetry).

Responses in the lesion projection zone were compared quantitatively with those in regions normally driven by intact retina using regions of interest defined anatomically to avoid any bias towards activation patterns. In both hemispheres, one region was selected at the occipital pole (OP), normally representing the central visual field, and another region in the fundus of the calcarine sulcus (CS), normally representing more peripheral locations. The BOLD signal plotted as a function of time shows robust modulations in response to stimulus onset at both the occipital pole and calcarine sulcus in controls (Fig. 1). Clear differences in the response latency of the signals measured at the occipital pole and calcarine sulcus reflect the normal retinotopic mapping of early visual areas. Fourier analysis was also applied to the average time series for each of the subjects presented in Figure 1. The resultant spectra (and associated Z-scores) are consistent with the time series, showing robust signals at the stimulation frequency at both cortical locations in controls, but only at the calcarine sulcus in the patients.

Group effects

The data analysis presented in Figure 1 captures responses in individuals and conforms to the approach used in previous work on a limited number of cases^{15,18,26}. Extending our analysis to the group level, participants were categorized according to age and visual status (young and elderly, patient and control). Responses were assessed at three cortical locations: the two mentioned above (CS and OP, shown in Fig. 1), and a third control region (CR) located further anterior in the brain in non-visual cortex, chosen to serve as a baseline measure.

The results for the elderly group are shown in Figure 2a. A two-way analysis of variance was performed with visual status (patient vs. control) and region of interest (CS vs. OP vs. CR) as main factors. A significant main effect was found for both visual status ($F = 8.62$, $p < 0.01$) and brain region ($F = 24.20$, $p < 10^{-6}$), with a significant interaction ($F=3.30$, $p < 0.05$). Post-hoc tests (corrected for multiple comparisons) revealed a significant difference between patients and controls at the occipital pole ($p < 0.01$), but none at the calcarine sulcus or at the control region. Within the patient group, signals at the occipital pole were not significantly different from the baseline measure at the control region, but were significantly different from signals from the intact retina at the calcarine sulcus ($p < 0.001$). Patient responses at the calcarine sulcus were robust and well above baseline ($p < 0.001$). In the control group,

signals at the occipital pole and calcarine sulcus were not significantly different from one another, but both differed significantly from the baseline response (CS vs. CR: $p < 0.001$; OP vs. CR: $p < 0.05$).

Previous work that revealed activity in the lesion projection zone primarily tested patients who acquired lesions earlier in adulthood than our patients with AMD. Comparing our JMD patients with the young control group, however, yielded the same results as in the elderly patients (Fig. 2b), with significant main effects of visual status ($F = 52.32, p < 10^{-7}$) and region of interest ($F = 95.72, p < 10^{-15}$) and a significant interaction between them ($F = 18.36, p < 10^{-5}$). Post-hoc tests (corrected) also revealed the same pattern of results as in the elderly groups, but with all differences achieving significance at $p < 0.001$. Large-scale remapping appears to be absent independent of the age in adulthood at which the retinal lesions are acquired.

To test the reproducibility of our results, we acquired additional data on a separate day in most participants ($N = 20/28$) and found that the data conformed to the same pattern. Repeated measures ANOVA revealed no main effect of session in all groups ($p > 0.05$). Combining data across sessions, we also tested explicitly for statistical differences associated with age across groups. A three-way ANOVA was performed on the elderly and young groups, with ROI, visual status, and age as factors. As in the individual age groups, significant main effects of visual status ($F = 23.40, p < 10^{-5}$) and ROI ($F = 60.00, p < 10^{-15}$) were found, as well as a significant interaction between them ($F = 7.18, p < 0.01$). There was also a main effect of age ($F = 8.82, p < 0.01$), a feature we have noted previously²⁷. However, there were no significant interactions between age and visual status ($F = 2.09, p = 0.15$) or age and ROI ($F = 2.31, p = 0.11$). Thus, although age affects the overall magnitude of fMRI responses, it does so similarly in both patients and controls, and does not alter the pattern of differences found between them.

Simulating retinal lesions in controls

Using a control region in a non-visual brain area as a baseline measure comes with the danger that small but genuine occipital signals may escape detection, for example, if signal-to-noise ratios vary across the brain²⁸, or if the control region is in fact responsive to visual stimuli. To improve specificity of our measurements, we compared signals within the same region of visual cortex (the occipital pole) in control subjects in the presence or absence of visual stimulation. Twelve new control subjects (mean age = 27) were scanned while passively viewing the expanding ring checkerboard stimulus either in full, or with a central mask (gray disk $radius = 7.5deg$) simulating a macular lesion. Figure 3 shows the superimposed response maps from a typical control participant in this experiment. The presence of the central mask in the stimulus largely removes significant responses from the occipital pole.

Using the new baseline measure, we compared responses from the new (young) control group with those from the young (age-matched) patients and controls from the first experiment, averaged across sessions (Fig. 4). A two-way ANOVA revealed main effects of group (patients vs. controls vs. new controls: $F = 38.57, p < 10^{-9}$) and region of interest (occipital pole vs. calcarine sulcus: $F = 56.08, p < 10^{-8}$), as well as a significant interaction between them ($F = 8.50, p < 0.001$). Post-hoc tests (corrected) showed that these effects were carried by important features at the occipital pole and calcarine sulcus. First, responses at the occipital pole did not differ significantly between patients and the new control group shown the simulated scotoma, but both were significantly below those of the original control

group shown the full stimulus ($p < 10^{-5}$ for both comparisons). Second, responses at the calcarine sulcus in all three groups are significantly above baseline, as expected. (Note also that patient responses at the calcarine sulcus fall significantly below those of the original age-matched controls, a point that will be addressed in the following section.) In summary, our results using an improved baseline measure again supports the absence of large-scale remapping in patients with MD.

Partial volume effects

Even though stimulation of peripheral retina is expected to produce fMRI responses of equal magnitude in both patients and controls, we note that signals at the calcarine sulcus are relatively reduced in both elderly and young patients (CS, Fig. 2) and significantly so when data were combined across sessions (Fig. 4). Because lesion size was variable across patients, the anatomically defined region of interest at the calcarine sulcus could include tissue within the lesion projection zone, effectively reducing the signal there. Such ‘partial volume’ effects are therefore predicted to be more likely when retinal lesions are large (e.g. see Fig. 6b, A8). A multiple regression was performed with lesion size (mean lesion diameter; see Table 1) and age as regressors, as age was shown previously to have a negative effect on fMRI responses (see above). The analysis revealed an overall significant relationship between lesion size, age, and response (coherence) at the calcarine sulcus ($R^2 = 0.308$, $p < 0.05$). Consistent with the partial volume prediction, the effect was carried entirely by lesion size ($t(\text{one-tailed}) = -1.95$, $p = 0.036$) rather than age ($t(\text{one-tailed}) = -0.74$, $p = 0.238$). In contrast, no such relationship was found in regions where no response was predicted and partial volume effects were less likely, either well within the lesion projection zone at the occipital pole ($R^2 = 0.059$, $p = 0.336$) or at the control region in non-visual cortex ($R^2 = 0.055$, $p = 0.346$).

Receptive field characteristics

While there are no significant group differences in occipital pole signals between patients and controls with simulated retinal lesions, there is a hint that in both groups occipital pole signals may exceed those found in the control region (Fig. 2). It is possible that these signals are visually driven by a small proportion of neurons with large and/or eccentric receptive fields^{19,29} that extend into areas of stimulated retina. To investigate the properties of potential visually driven signals, we modeled population receptive fields³⁰ of responses within an enlarged region centered on the OP region described above (see Methods). For a description of how neural and population receptive field are considered in the context of the work reported here please see Supplementary Material. Figure 5 shows that indeed, the mean population receptive field location (a) and size (b) around the occipital pole are abnormally large in both patients (location: $t = 3.81$, $p < 0.001$; size: $t = 2.90$, $p = 0.01$) and controls when central retinal lesions are simulated (location: $t = 7.90$, $p < 0.001$; size: $t = 2.44$, $p = 0.032$). The significant shift in population receptive field location (Fig. 5a) implies an apparent shift in the representation of these voxels, i.e. rendering them ‘ectopic’. In contrast, population receptive fields within the calcarine sulcus region (Fig. 5, bottom row) did not differ significantly either between patient and control groups (location: $t = 1.09$, $p = 0.285$; size: $t = 0.72$, $p = 0.481$) or between masked and unmasked conditions for the controls (location: $t = 0.84$, $p = 0.414$; size: $t = 0.44$, $p = 0.669$). Fixation instability in patients cannot account for the effects observed, because 1) patients and controls with

simulated lesions show similar results and 2) both the occipital pole and calcarine sulcus regions would be affected⁵, which they clearly are not.

Cortical representation

Using phase encoded stimuli also allows the cortical mapping of retinal coordinates to be assessed at an individual level. Figure 6 shows fMRI response maps in the occipital lobes of several individuals in the elderly and young groups. While subjects with normal vision show complete retinal representations throughout the occipital lobes (Fig 6a), patients with macular degeneration show response maps that are consistent with the projection from intact parts of retina only (Fig 6b). Furthermore, the extent of activation and its phase (shown in color) reflect the size of the spared retina. A large retinal lesion results in a smaller activation area on the brain (e.g. A8) and *vice versa* (e.g. J2).

To compare cortical maps quantitatively, we measured the area of activity within the primary visual cortex, A_M , for each patient and control participant with simulated lesions and compared it with a mean predicted area, \bar{A}_p , based on the patient's scotoma and normal mappings of age-matched controls (see Methods and Figure 7). The ratio A_M / \bar{A}_p is compared across participant groups in Figure 7 and reveals no significant effect of group ($F = 0.81$, $p = 0.46$). Moreover, all groups exhibited ratios that were no different from unity (AMD: $t = 0.59$, $p = 0.57$; JMD: $t = -0.55$, $p = 0.60$; Controls: $t = 1.93$, $p = 0.08$) an indication that the area of primary visual cortex activated in all participant groups can be predicted on the basis of normal retinotopic maps. Because each ratio was computed with age-matched control data, patient groups were combined to increase statistical power, but still yielded no significant difference between patients and controls ($t = -0.81$, $p = 0.41$) or difference from unity in the ratio ($t = 0.14$, $p = 0.89$). Given the variance for patient and control groups in our ratio measure, a significant (at $p < 0.05$) difference in the ratio (of 0.23) would occur if the mean increase in cortical area compared to controls exceeded 160mm^2 in each hemisphere. This is relatively small compared to the total area of primary visual cortex ($\sim 2500\text{mm}^2$ - see³¹). Our analysis provides strong, quantitative evidence that the extent of early visual cortical activity in patients and lesion controls can be predicted on the basis of normal retinotopic maps.

DISCUSSION

Seminal work on early visual deprivation in animals has shown that visual cortex can develop to devote more of its territory to intact visual input at the expense of its representation of impoverished input³²⁻³⁵. Such reallocation of cortical processing has also been demonstrated when early visual areas remap following congenital retinal lesions in human⁶. In adulthood the cortex is less plastic, but even so, remapping of the visual cortical representation has been inferred on the basis of ectopic receptive fields in the lesion projection zone in animal models⁷⁻¹³. This effect is however rather modest and has been called into question recently¹⁹. Even so, recent literature on human adults^{15,26} suggests a large-scale extension of remapping of the type reported in animal models. We aimed to test explicitly whether or not visual cortical mapping changes following retinal lesions in adult humans. Our results indicate that it does not in three different ways.

First, we find that at the occipital pole, a cortical location that we are certain lies within the lesion projection zone, the signals observed in patients are no different than those found in control participants in whom we simulated a central scotoma. The spatially specific region of interest analysis has been used extensively in previous research^{15,26} and has been shown to be highly sensitive to remapping⁶. Our result runs contrary to the view that the occipital pole in V1 takes on a new mapping to respond strongly to peripheral stimuli in a way that differs from normal. The previous work in this area has been limited to small numbers of patients and control participants^{15,26}. Moreover, previous work has used task-stimulus combinations^{15,26} that produced widespread signals in the lesion projection zone in patients but less in controls, most likely as a result of feedback from extrastriate cortex rather than remapping¹⁸.

Second, our results show clearly that throughout the lesion projection zone there are voxels with 'ectopic' receptive fields, but they are equally common and represent the same regions of visual field in both patients and controls. This novel finding speaks more generally to the way in which ectopic receptive fields should be interpreted. Frequently, the existence of ectopic receptive fields has been taken as evidence for remapping⁷⁻¹³. That ectopic characteristics can be recorded from normally sighted controls challenges this notion, particularly in the context of fMRI research^{15,26}. Furthermore, we showed that voxels with ectopic receptive fields were not restricted to the fringe of the lesion projection zone, where most electrophysiological measurements have been taken⁷⁻¹³. We propose, like others^{19,30}, that each cortical location (voxel) contains many neurons, the responses of which can be influenced by stimuli at a range of locations, but that the overall population response is heavily weighted to a modal location. If stimuli are presented only to locations that are a considerable distance from this modal location, the responses of the voxel will be weak but could be driven by neurons with receptive fields that are large, displaced or large and displaced (see Supplementary material). We found that only 5-7% of voxels in the lesion projection zone could be classified as responsive, meaning that such signals could escape detection with conventional analyses that average signals over the whole region of interest. Interestingly, the probability of detecting a voxel with ectopic receptive fields is similar to the probability of detecting a neuron with ectopic receptive fields¹³. The ectopic signals in the lesion projection zone may originate from various sources, including feedback³⁶⁻³⁸ and lateral connections^{39,40}. Task-specific feedback could elicit more activity in the lesion projections zone in patients than in controls because of the absence of feedforward signals in patients¹⁸. Nevertheless, our results indicate that there is no need to invoke remapping as an explanation of responses in V1 of patients.

Third, our work has, for the first time, been able to perform a quantitative assessment of the area of cortex driven by intact retina in patients with retinal disease. Limited size of patient and control groups coupled with the well-known large variance in visual cortical area across participants^{31,41} has prevented such an analysis in previous studies. Our results show that the representation of the visual field in V1 in patients can be predicted accurately on the basis of normal retinotopic mapping and that no significant remapping or reorganization was evident. The measures we derived are sensitive to relatively small changes in cortical maps (<6.5% of V1). This allows us to conclude that there is no remapping of visual cortex over the scale seen in those with congenital central retinal lesions⁶. If neural responses change over time within a very small strip of cortex on the edge of the lesion projection zone, as some have

proposed for animal models ⁷⁻¹³, this could escape detection with our analysis. However, we are principally concerned with a large-scale extension of this type of remapping, which we conclude does not exist in humans with central retinal lesions acquired in adulthood.

In line with our results, some previous studies on individuals have also found no evidence of remapping of primary visual cortex following retinal damage. A study using cytochrome oxidase to measure activity in an individual with macular degeneration and in macaque models of visual deafferentation found no long term changes in primary visual cortical organization ⁴². Using fMRI and retinotopic mapping methods similar to our own, no activation was found in the lesion projection zone in another patient with macular degeneration ¹⁴. It has been proposed that this negative result could be due to the spared foveal vision this patient exhibited ²⁶. With this in mind, we only included patients with central lesions without foveal sparing. A combined fMRI and multi-unit neurophysiological study in a carefully controlled animal model (homonymous retinal, but not macular, lesions induced in adult macaques) also showed no long-term changes that would indicate remapping of visual cortex ²⁵. A recent report of a case series of four patients with age-related macular degeneration and four with the juvenile form also indicates limited reorganization, but explicit mapping experiments to assess group differences in cortical mapping quantitatively were not undertaken ⁴³. Having assessed retinotopic maps quantitatively in sixteen patients, we are confident that the absence of cortical remapping following retinal lesions in adulthood is a general finding.

The stability of visual organization we observe may prove to be beneficial. Many of the most promising treatments aimed at restoring vision at the retinal level, such as anti-angiogenic injections, retinal prosthetics and stem-cell therapy, rely on the assumption that cortical circuitry remains largely unchanged. That we can detect no functional abnormality in the visual cortex of patients is reassuring. However, the long term removal of the principal input to visual cortex can give rise to a reduction in cortical volume⁴⁴. It remains to be seen, therefore, if neurons in the lesion projection zone can process input normally once it is restored.

METHODS

Participants. Patients: Eight patients with stabilized age-related macular degeneration (AMD) (ages 70-90) and a further eight with the juvenile form of macular degeneration (Stargardt's Disease) (ages 19-49) were recruited at the Moorfields Eye Hospital, London. All patients had established bilateral lesions for at least 1 year, with a central scotoma of less than 10 deg radius spanning the fovea and a stable preferred retinal locus (PRL). Visual field sensitivity and fixation ability for all patients were evaluated directly on the retina using an MP1 microperimeter (NIDEK Co. Ltd., Italy). Location of the foveal center, PRL coordinates and fixation stability (bivariate contour ellipse area of fixation measurements) were determined using methods outlined in Timberlake et al. (2005). The mean diameter of the absolute retinal lesion was also computed from the microperimetry maps. Control participants: Five age matched-participants (ages 61-77) were recruited as controls for the AMD group and seven age matched-participants (ages 18-37) as controls for the JMD group. A further 12 control participants (ages 18-41) were recruited for a follow up experiment simulating retinal lesions. All control participants had normal or corrected-to-normal vision. Experimental protocols were approved by the London Multicenter Research Ethics Committee, Royal Holloway University of London Ethics Committee and the York Neuroimaging Center Science and Ethics Committee.

Scanning. Functional and structural MRI data were acquired using 8-channel, phase-array head coils on either a Siemens Trio 3 Tesla at the Combined Universities Brain Imaging Center (CUBIC, Royal Holloway, University of London), or on a GE 3-Tesla Signa HD Excite scanner at the York Neuroimaging Center (YNiC, University of York).

Structural data: Multi-average, whole-head T1-weighted anatomical volumes were acquired for each participant (1.0 - 1.13mm³ isotropic). Sequences used were 3D-MDEFT on the Siemens Trio or 3D-FSPGR on the GE Signa; imaging parameters in both sequences provide good gray-white contrast allowing the segmentation of anatomical data into gray and white matter, and subsequent visualization in volume and inflated cortical views.

Functional data: Gradient recalled echo pulse sequences were used to measure T2* BOLD data (TR=3000ms, TE=30ms, FOV=28.8cm, 128x128 matrix, 25 contiguous slices with 3mm slice thickness). Images were read out using an EPI sequence. Magnetization was allowed to reach a steady state by discarding the first five volumes, an automated feature on both the scanners used.

Stimuli. Computer-generated visual stimuli were presented using a LCD projector (Sanyo PLC-XP40L at Royal Holloway University of London, Dukane ImagePro 8942 at the University of York); stimuli were rear projected onto an acrylic screen situated in the bore of the MRI scanner, behind the participant's head. Participants viewed the stimuli via a mirror mounted on the head coil. Standard retinotopic mapping stimuli were used: a rotating wedge to map polar angle, and an expanding annulus to map eccentricity²¹⁻²⁴. Stimuli were generated with MATLAB and controlled by MatVis (Neurometrics Institute, Oakland, CA). All stimuli were unmasked portions of a 100% contrast radial checkerboard with 8 rings and 24 radial segments on a mean gray background. Contrast reversal rate was 6 Hz. Each scan contained either the expanding annulus or rotating wedge. Projector throw was adjusted to stimulate the central 30deg x 30deg of visual angle (15 deg radius). The wedge stimulus was a 90 deg wedge of the

flickering checkerboard, rotating about the center of the screen. The ring stimulus comprised 3 rings of the checkerboard which increased in angular extent (to a maximum of 15 deg) as it moved out from the center of the visual field; each ring was replaced by a new ring at the center as the existing ring approached the edge of the visual field. Both the wedge and ring stimuli had a period of 36 seconds and were repeated for 7 full cycles.

Experiment 1. The standard expanding ring and rotating wedge stimuli described above were used. In addition, the position of a red fixation cross was manipulated to ensure that stimuli were centered on each individual participant's retina. For control participants, a red fixation cross was placed at the center of the stimulus. For patients, the cross was placed at each individual's stable preferred retinal locus, as measured by microperimetry. Four ring and four wedge datasets were typically collected for each participant during a single visit, except where participant discomfort or excessive movement required fewer scans. Only three scans were collected during the first session in two AMD patients and two JMD patients, and only two scans were performed on one of the elderly controls. Scans were repeated in a second visit in most participants (20 out of 28). Four scans were again performed during the second session, except in two AMD patients (3 scans) and four JMD patients (three had 3 scans, one had 2 scans).

Experiment 2. As in Experiment 1, standard retinotopic mapping stimuli were used. A red fixation cross was placed in the center of the stimulus. In separate scans, the 12 control participants were either shown the full stimulus (ring and wedge), or a masked version (of the rings) to simulate a central lesion. The mask consisted of a centrally placed static disk (7.5 deg radius) at mean luminance gray such that the central portion of the visual field was constant throughout the scan (Fig. 3). At least two scans were acquired for each condition. Ten of the 12 participants returned for a second scanning session on a separate date.

Data analysis. Data were analyzed using publicly available tools (<http://white.stanford.edu/software/>). Most data analysis was performed in MATLAB (The Mathworks, Natick, MA, USA) using the mrVISTA toolbox.

1. Anatomical data. The occipital cortices of acquired anatomical volumes were manually segmented into white and gray volumes (mrGray)⁴⁵. The cortical surface (gray matter) of each subject was constructed and rendered in 3D from this segmentation using mrMesh/mrVista⁴⁶.
2. Functional data. Functional images were corrected for spatial inhomogeneity (mrInitRet). Motion correction was achieved using FSL's MCFLIRT⁴⁷. Functional time series were high-pass filtered to remove baseline drifts. Percent signal change was computed for each voxel by dividing by and subtracting its mean amplitude value over time. The strength of stimulus-synchronized activity at each voxel was assessed using coherence. Coherence (C) is defined as the Fourier amplitude of the BOLD signal at the stimulus fundamental frequency ($f_0 = 7$) divided by the sum of amplitudes of frequency bins around the fundamental ($C = A(f_0) / \sum (A(f)^2)^{1/2}$)^{18,25}. The visual field representation of each voxel in cortex was derived by using the Fourier phase at the stimulus frequency, corresponding to the relative delay of the cyclical response^{22,48}. Functional data were averaged across scans for repeated scans

(usually 4) within a session for each individual. Functional data were manually aligned to the high-resolution anatomical volume and visualized in 3D.

3. ROI analysis. Regions of interest (ROIs) were defined by an algorithm that gathered all contiguous gray matter within a circular patch 8mm in diameter centered on a selected point within the high resolution structural data. Three ROIs were chosen in each hemisphere of each participant based strictly on anatomical criteria - one at the occipital pole (OP) to represent activity from the fovea (the lesion projection zone in patients), one more anterior within the calcarine sulcus (CS) to represent activity from more peripheral retina (which is intact in patients) and one further anterior in the brain on the lateral aspect of the frontal lobes, serving as a control region (CR) in the first experiment. The mean coherence was calculated across voxels within an ROI for each individual and averaged across scans within each session. The fMRI noise distribution is not normal and may differ from one individual to the next or from one day to the next. To normalize the responses, therefore, the logarithm of the resulting coherence data was taken prior to averaging data across scanning sessions and across participants⁴⁹.

4. Population receptive field analysis. We assessed the degree to which the time series of any voxel in predefined regions of interest in the gray matter fitted a series of receptive field models as described by Dumoulin et al.³⁰. Best fitting models were retained if they accounted for more than 15% of the variance of the time series of each voxel as in previous research⁵⁰. The retained models were then averaged across voxels to give an overall measure of the population receptive field properties for each region of interest. The data used for modelling were for the expanding ring stimuli only because it was for this presentation that we had a comparable number of runs across the participant groups, and it was the only stimulus that was masked to simulate retinal lesions. It is important to note that the candidate models were identical for all stimulus conditions and we did not restrict the receptive field models to any locations or sizes. The regions of interest considered were CS, as specified above, and OP, but in this case the diameter of OP was 20mm to gain increased sensitivity. While the 20mm diameter region of interest might capture some signals from tissue receiving input from intact retina in patients with small retinal lesions, we ensured that for the control participants receiving full-field and simulated lesion stimulation, the OP ROI only included voxels responding to eccentricities less than 7.5deg when the full stimulus was presented.

5. Cortical area computations. We computed the area of primary visual cortex, A_M , that exhibited activity above a coherence threshold of 0.30 for all patients and in controls in whom we simulated retinal lesions. Using responses to rotating wedge stimuli, we first identified the cortical representations of the upper and lower vertical meridians marking the boundaries of V1 in each participant (see Figure 7). We then defined a V1 region of interest that was bounded by the extrapolation of the vertical meridians to the occipital pole and an anterior boundary that was just beyond the limit of activity in response to rotating wedges. This region was not restricted to those voxels that exceeded a specific threshold, but rather was a generously defined estimate of the extent of V1. Voxels within this V1 region that responded to rings at a coherence of greater than 0.30 were retained for the calculation of the area of significant activity in V1. The cortical area of activity was calculated using the methods described by Dougherty et al.⁴¹. We then computed a series of estimates of the predicted area of activation, A_p , based on the intact regions of visual field in patients (see Figure 7 for a schematic of the method). For each patient we computed estimates from the corresponding group of age-matched controls (e.g. for each JMD patient we obtained 7 estimates one from each of the young

control subjects). The mean predicted area, \bar{A}_p , was then computed. We repeated these computations to obtain \bar{A}_p for controls with simulated central visual loss. Note that these computations were also based on the original data from the young control subjects. If remapping were to occur, A_M will exceed \bar{A}_p and thus a ratio of the A_M to \bar{A}_p will exceed unity. Using the ratio as our outcome measure is essential because it accounts for individual differences in retinal lesion size.

6. Statistical analyses. Statistics were calculated using functions in the MATLAB Statistical Toolbox. A two-way analysis of variance was performed on the averaged expanding ring data (for each session) for the elderly group and for the young group. Visual status (patient vs. control) and region of interest (OP vs. CS vs. CR) were the independent variables and log coherence (fMRI response magnitude) was the dependent variable. A repeated measures ANOVA was performed on the data to test for significant differences within subjects across two sessions. To test for age effects, a three-way analysis of variance was performed on the combined data, with age, visual status and region of interest as factors. All ANOVAs employed a Type III sum of squares calculation, and all subsequent multiple comparisons were corrected using the Tukey-Kramer criterion, as appropriate for an unbalanced design with unequal number of subjects across groups. A multiple regression analysis was performed on the patient data to determine the effects of lesion size and age on log coherence responses for each ROI. For the receptive field analysis, we used Student *t* tests to evaluate group differences in eccentricity and size of the receptive fields and sampling probability at each cortical location. Linear regression was used to assess the relationship between eccentricity and size of population receptive fields in the OP region of interest; 95% confidence intervals in the linear correlation parameters was estimated using jackknife resampling, taking into consideration the unequal number of points contributed by each participant. For the cortical area measures in Figure 7, group effects and deviations of the area ratio from unity were evaluated using *t* tests and ANOVAs, respectively.

ACKNOWLEDGEMENTS

We would like to thank all of our participants. We are also grateful to the Medical Research Council for funding this study (G0401339). KVH and FWC were supported by a grant from Stichting Nederlands Oogheelkundig Onderzoek and by European Union grants #043157 (Syntex) and #043261 (Percept). AT, GSR and MDC also received financial support from the Department of Health through an award made by the National Institute for Health Research to Moorfields Eye Hospital NHS Foundation Trust and UCL Institute of Ophthalmology for a Specialist Biomedical Research Centre for Ophthalmology. The views expressed in this publication are those of the authors and not necessarily those of the NHS, the National Institute for Health Research, the Department of Health or the EU commission. We thank Edward Silson for constructive discussion of the manuscript.

REFERENCES

1. Wandell, B.A., Dumoulin, S.O. & Brewer, A.A. Visual field maps in human cortex. *Neuron* **56**, 366-83 (2007).
2. Morland, A.B., Baseler, H.A., Hoffmann, M.B., Sharpe, L.T. & Wandell, B.A. Abnormal retinotopic representations in human visual cortex revealed by fMRI. *Acta Psychol (Amst)* **107**, 229-47. (2001).
3. Hoffmann, M.B., Tolhurst, D.J., Moore, A.T. & Morland, A.B. Organization of the visual cortex in human albinism. *J Neurosci* **23**, 8921-30 (2003).
4. Muckli, L., Naumer, M.J. & Singer, W. Bilateral visual field maps in a patient with only one hemisphere. *Proc Natl Acad Sci U S A* **106**, 13034-9 (2009).
5. Levin, N., Dumoulin, S.O., Winawer, J., Dougherty, R.F. & Wandell, B.A. Cortical maps and white matter tracts following long period of visual deprivation and retinal image restoration. *Neuron* **65**, 21-31.
6. Baseler, H.A. et al. Reorganization of human cortical maps caused by inherited photoreceptor abnormalities. *Nat Neurosci* **5**, 364-70 (2002).
7. Kaas, J.H. et al. Reorganization of retinotopic cortical maps in adult mammals after lesions of the retina. *Science* **248**, 229-31 (1990).
8. Heinen, S.J. & Skavenski, A.A. Recovery of visual responses in foveal V1 neurons following bilateral foveal lesions in adult monkey. *Exp Brain Res* **83**, 670-4 (1991).
9. Chino, Y.M., Kaas, J.H., Smith, E.L., 3rd, Langston, A.L. & Cheng, H. Rapid reorganization of cortical maps in adult cats following restricted deafferentation in retina. *Vision Res* **32**, 789-96 (1992).
10. Gilbert, C.D. & Wiesel, T.N. Receptive field dynamics in adult primary visual cortex. *Nature* **356**, 150-2 (1992).
11. Darian-Smith, C. & Gilbert, C.D. Topographic reorganization in the striate cortex of the adult cat and monkey is cortically mediated. *J Neurosci* **15**, 1631-47 (1995).
12. Kaas, J.H. Sensory loss and cortical reorganization in mature primates. *Prog Brain Res* **138**, 167-76 (2002).
13. Giannikopoulos, D.V. & Eysel, U.T. Dynamics and specificity of cortical map reorganization after retinal lesions. *Proc Natl Acad Sci U S A* **103**, 10805-10 (2006).
14. Sunness, J.S., Liu, T. & Yantis, S. Retinotopic mapping of the visual cortex using functional magnetic resonance imaging in a patient with central scotomas from atrophic macular degeneration. *Ophthalmology* **111**, 1595-8 (2004).
15. Baker, C.I., Peli, E., Knouf, N. & Kanwisher, N.G. Reorganization of visual processing in macular degeneration. *J Neurosci* **25**, 614-8 (2005).
16. Schumacher, E.H. et al. Reorganization of visual processing is related to eccentric viewing in patients with macular degeneration. *Restor Neurol Neurosci* **26**, 391-402 (2008).
17. Cowey, A. & Walsh, V. Magnetically induced phosphenes in sighted, blind and blindsighted observers. *Neuroreport* **11**, 3269-73 (2000).
18. Masuda, Y., Dumoulin, S.O., Nakadomari, S. & Wandell, B.A. V1 projection zone signals in human macular degeneration depend on task, not stimulus. *Cereb Cortex* **18**, 2483-93 (2008).
19. Wandell, B.A. & Smirnakis, S.M. Plasticity and stability of visual field maps in adult primary visual cortex. *Nat Rev Neurosci* **10**, 873-84 (2009).
20. Masuda, Y. et al. Task-dependent V1 responses in human retinitis pigmentosa. *Investigative Ophthalmology and Visual Science*. **51**, 5356-5364 (2010).
21. DeYoe, E.A. et al. Mapping striate and extrastriate visual areas in human cerebral cortex. *Proc Natl Acad Sci U S A* **93**, 2382-6 (1996).

22. Engel, S.A., Glover, G.H. & Wandell, B.A. Retinotopic organization in human visual cortex and the spatial precision of functional MRI. *Cereb Cortex* **7**, 181-92 (1997).
23. Engel, S.A. et al. fMRI of human visual cortex [letter] [published erratum appears in Nature 1994 Jul 14;370(6485):106]. *Nature* **369**, 525 (1994).
24. Sereno, M.I. et al. Borders of multiple visual areas in humans revealed by functional magnetic resonance imaging [see comments]. *Science* **268**, 889-93 (1995).
25. Smirnakis, S.M. et al. Lack of long-term cortical reorganization after macaque retinal lesions. *Nature* **435**, 300-7 (2005).
26. Baker, C.I., Dilks, D.D., Peli, E. & Kanwisher, N. Reorganization of visual processing in macular degeneration: replication and clues about the role of foveal loss. *Vision Res* **48**, 1910-9 (2008).
27. Crossland, M.D., Morland, A.B., Feely, M.P., von dem Hagen, E. & Rubin, G.S. The effect of age and fixation instability on retinotopic mapping of primary visual cortex. *Invest Ophthalmol Vis Sci* **49**, 3734-9 (2008).
28. Parrish, T.B., Gitelman, D.R., LaBar, K.S. & Mesulam, M.M. Impact of signal-to-noise on functional MRI. *Magn Reson Med* **44**, 925-32 (2000).
29. Cavanaugh, J.R., Bair, W. & Movshon, J.A. Nature and interaction of signals from the receptive field center and surround in macaque V1 neurons. *J Neurophysiol* **88**, 2530-46 (2002).
30. Dumoulin, S.O. & Wandell, B.A. Population receptive field estimates in human visual cortex. *Neuroimage* **39**, 647-60 (2008).
31. Andrews, T.J., Halpern, S.D. & Purves, D. Correlated size variations in human visual cortex, lateral geniculate nucleus, and optic tract. *J Neurosci* **17**, 2859-68 (1997).
32. Hubel, D.H. & Wiesel, T.N. The period of susceptibility to the physiological effects of unilateral eye closure in kittens. *J Physiol (Lond)* **206**, 419-36 (1970).
33. Hubel, D.H., Wiesel, T.N. & LeVay, S. Plasticity of ocular dominance columns in monkey striate cortex. *Philos Trans R Soc Lond B Biol Sci* **278**, 377-409 (1977).
34. LeVay, S., Wiesel, T.N. & Hubel, D.H. The development of ocular dominance columns in normal and visually deprived monkeys. *J Comp Neurol* **191**, 1-51 (1980).
35. Horton, J.C. & Hocking, D.R. Timing of the critical period for plasticity of ocular dominance columns in macaque striate cortex. *J Neurosci* **17**, 3684-709 (1997).
36. Williams, M.A. et al. Feedback of visual object information to foveal retinotopic cortex. *Nat Neurosci* **11**, 1439-1445 (2008).
37. Angelucci, A. & Bullier, J. Reaching beyond the classical receptive field of V1 neurons: horizontal or feedback axons? *J Physiol Paris* **97**, 141-54 (2003).
38. Angelucci, A. & Sainsbury, K. Contribution of feedforward thalamic afferents and corticogeniculate feedback to the spatial summation area of macaque V1 and LGN. *J Comp Neurol* **498**, 330-51 (2006).
39. Lund, J.S. Anatomical organization of macaque monkey striate visual cortex. *Annu Rev Neurosci* **11**, 253-88 (1988).
40. Gilbert, C.D. & Wiesel, T.N. Morphology and intracortical projections of functionally characterised neurones in the cat visual cortex. *Nature* **280**, 120-5 (1979).
41. Dougherty, R.F. et al. Visual field representations and locations of visual areas V1/2/3 in human visual cortex. *J Vis* **3**, 586-98 (2003).
42. Horton, J.C. & Hocking, D.R. Monocular core zones and binocular border strips in primate striate cortex revealed by the contrasting effects of enucleation, eyelid suture, and retinal laser lesions on cytochrome oxidase activity. *J Neurosci* **18**, 5433-55 (1998).
43. Liu, T. et al. Incomplete cortical reorganization in macular degeneration. *Invest Ophthalmol Vis Sci* (2010).

44. Boucard, C.C. et al. Changes in cortical grey matter density associated with long-standing retinal visual field defects. *Brain* **132**, 1898-906 (2009).
45. Teo, P.C., Sapiro, G. & Wandell, B.A. Creating connected representations of cortical gray matter for functional MRI visualization. *IEEE Trans Med Imaging* **16**, 852-63 (1997).
46. Wandell, B.A., Chial, S. & Backus, B.T. Visualization and measurement of the cortical surface. *J Cogn Neurosci* **12**, 739-52. (2000).
47. Jenkinson, M., Bannister, P., Brady, M. & Smith, S. Improved optimization for the robust and accurate linear registration and motion correction of brain images. *Neuroimage* **17**, 825-41 (2002).
48. Wandell, B.A., Brewer, A.A. & Dougherty, R.F. Visual field map clusters in human cortex. *Philos Trans R Soc Lond B Biol Sci* **360**, 693-707 (2005).
49. Lewis, S.M. et al. Logarithmic transformation for high-field BOLD fMRI data. *Exp Brain Res* **165**, 447-53 (2005).
50. Winawer, J., Horiguchi, H., Sayres, R.A., Amano, K. & Wandell, B.A. Mapping hV4 and ventral occipital cortex: the venous eclipse. *J Vis* **10**(2010).

ID	Diagnosis	Sex	Age (years)	Eye tested	Lesion diameter (μ)	Acuity (logMAR)	BCEA ($^{\circ}$)
A1	AMD	F	90.9	Right	9	0.92	17.7
A2	AMD	F	83.5	Right	8	0.98	12.43
A3	AMD	F	81.8	Left	7	0.54	17.7
A4	AMD	M	76.3	Left	6	0.36	8.26
A5	AMD	M	80.2	Left	10	1.06	15.16
A6	AMD	F	70.8	Left	4	0.9	12.37
A7	AMD	M	83.8	Left	15	0.86	20.37
A8	AMD	M	80.6	Right	13	0.76	5.33
J1	Stargardt's	M	19.8	Left	5	0.74	11.71
J2	Stargardt's	F	19.7	Left	3	1.02	2.24
J3	Stargardt's	M	49.5	Right	6	0.56	14.47
J4	Stargardt's	F	41.2	Right	10	0.9	1.69
J5	Stargardt's	F	34.7	Right	8	1.08	13.54
J6	Stargardt's	F	39.4	Right	9	0.98	18.11
J7	Stargardt's	F	24.3	Left	3.5	0.66	9.33
J8	Stargardt's	M	35.8	Left	17	1.12	13.26

Table 1: Summary of patients in the study. AMD = bilateral age-related macular degeneration; logMAR = log(minimum angle of resolution); BCEA = bivariate contour ellipse area, a measure of fixation ability using microperimetry.

FIGURE CAPTIONS

Figure 1: Cortical responses to visual stimulation. BOLD responses for 4 individuals (from left to right): a young control subject (YC4, age 30), a young patient (J3, age 49), an elderly control subject (EC5, age 66) and an elderly patient (A6, age 70). Visual field results from microperimetry for each patient are inset to the right of each brain image and indicate absolute (black) and partial (gray) scotoma. Dotted concentric circles represent 5, 10 and 15 deg eccentricity. BOLD response coherence is encoded in colour and superimposed on smoothed, left occipital lobes. Single cycle time series averages are shown for the two occipital regions of interest representing central (OP, occipital pole) and more peripheral retina (CS, calcarine sulcus). Fast Fourier Transforms were performed on each full time series, and amplitude spectra are also shown for each ROI; stimulus frequency (7 cycles/scan) is indicated by the red dot. Z-scores indicate the number of standard deviations the FFT amplitude at the stimulus frequency differs from the distribution of all of the other frequency amplitudes.

Figure 2: Mean coherences for each region of interest, averaged across individuals for each group (OP=occipital pole; CS=calcarine sulcus; CR=control region in non-visual cortex). Error bars indicate standard error. *** = $p < 0.001$; ** = $p < 0.01$; * = $p < 0.05$. **(a)** Elderly patients (AMD) vs. elderly controls. **(b)** Young patients (JMD) vs. young controls.

Figure 3: Simulating retinal lesions in a control subject. In both panels the left occipital lobe of a control subject is shown with BOLD signal coherence superimposed on the surface. Below each panel time series (averaged to a single stimulus cycle) and amplitude spectra of the time series are given for circular regions of cortex at the occipital pole (OP) and calcarine sulcus (CS). **(a)** Response to expanding checkerboard ring stimulus spanning full field. **(b)** Response to same stimulus as in (a), but with central +/- 7.5 deg masked with a uniform, mean luminance gray disc. Details as in Fig. 1.

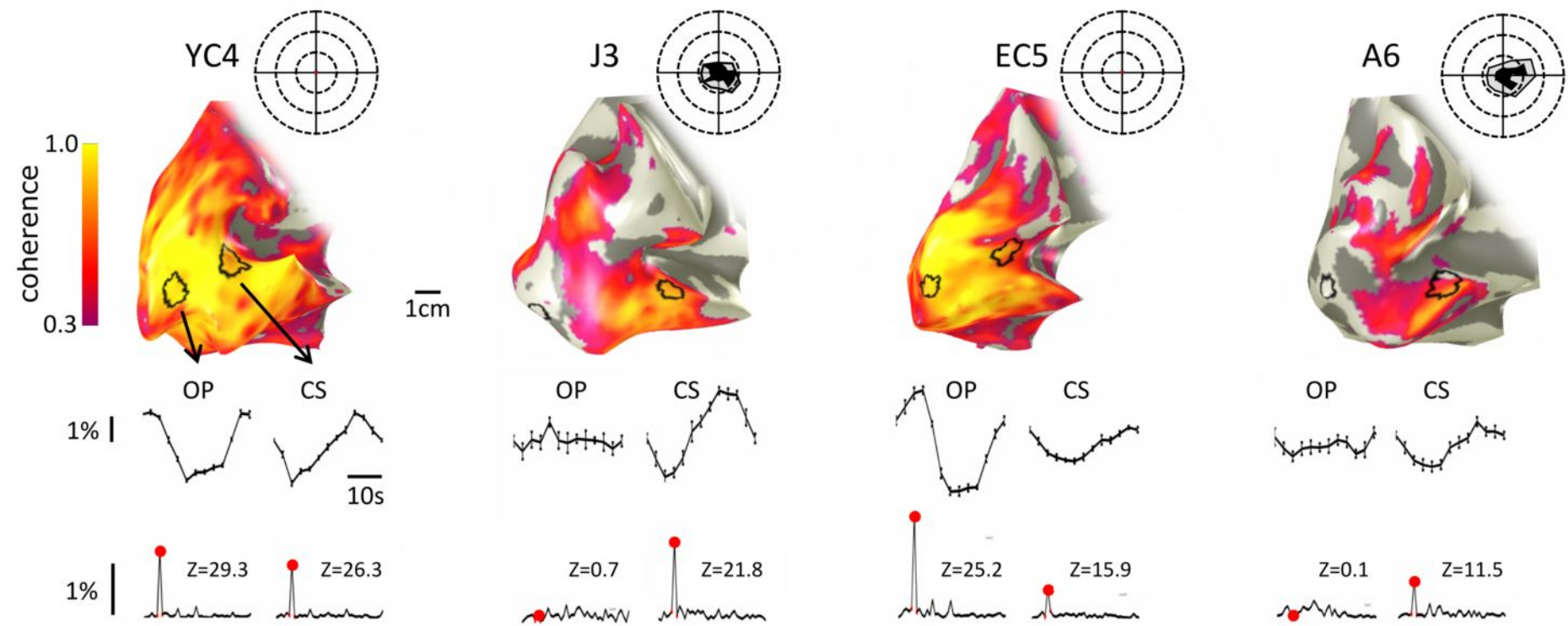
Figure 4: Occipital lobe responses compared across groups and regions of interest. Mean coherences averaged across sessions and across individuals from three groups: (1) Young patient data from Experiment 1, (2) Young control data from Experiment 1 and (3) Lesion control group data from Experiment 2 using new baseline measure at the occipital pole (OP) in response to stimulus with central +/- 7.5 deg masked with uniform gray. CS=calcarine sulcus. *** = $p < 0.001$; ** = $p < 0.01$; * = $p < 0.05$.

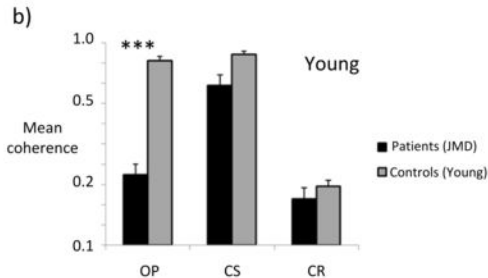
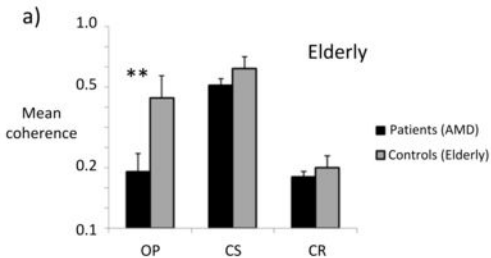
Figure 5: Population receptive field (pRF) characteristics in the lesion projection zone (a) and the calcarine sulcus (b). Mean pRF locations and sizes, and the sampling probability (percent voxels exceeding 15% variance explained) are shown in the three plots from left to right. Light gray bars show data for MD patients and age-matched controls. Data are given for combined age groups, because none of the outcome measures showed group contrasts (patients vs controls) that were specific to age (location: $F = 0.27$, $p = 0.603$; size: $F = 3.36$, $p = 0.074$; sampling probability: $F = 0.27$, $p = 0.603$). In two patients we were unable to derive population receptive field estimates in the lesion projection zone. Dark gray bars show data for controls presented the unmasked (100%) stimulus or the stimulus simulating a central scotoma (50% masked). Stars indicate significance at $p < 0.05$ (one star) and $p < 0.001$ (three stars).

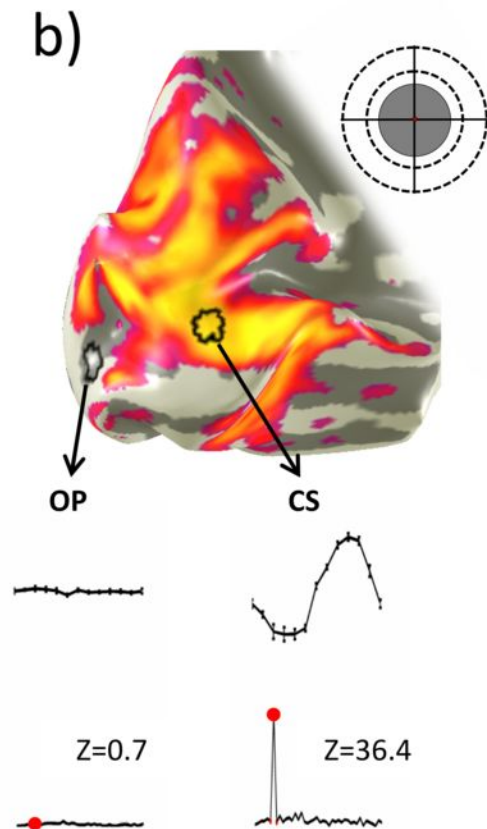
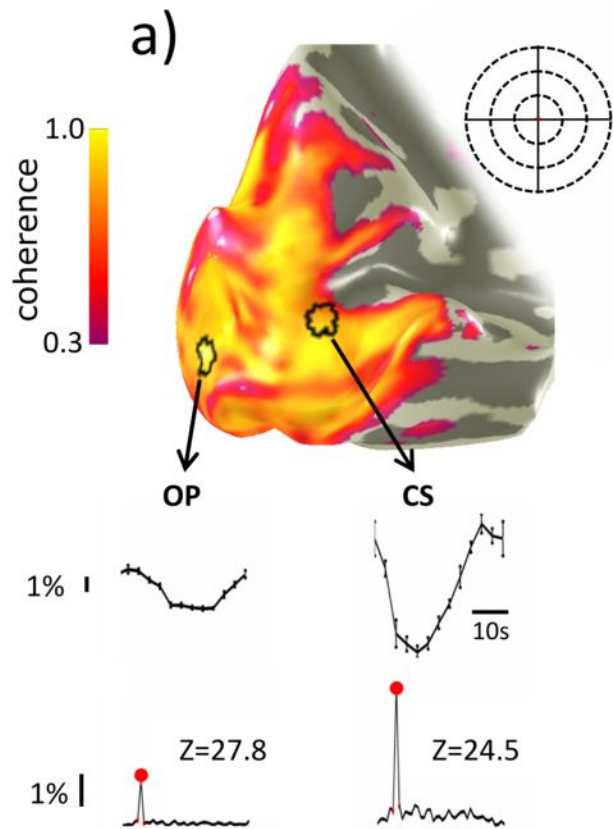
Figure 6: Individual eccentricity maps. fMRI response maps of visual eccentricity superimposed on individual left, partially inflated, occipital lobes for control subjects **(a)** and six individual patients **(b)**. False color is used to indicate the position on the retina (see semi-circular key) that the cortex is responsive to. In **(b)** filled black regions of the semicircular key indicate the absolute retinal lesion (scotoma), while outlined region exhibits significant, but not absolute loss of vision. The patients'

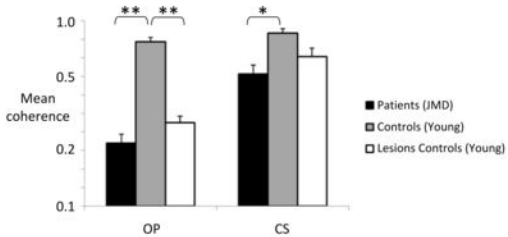
cortical maps are presented in ascending order (from left to right starting on the top row) of mean lesion diameter (MLD). The cortical representations closely correspond to the spared retina. Indeed even retinal locations with reduced sensitivity elicit activity. In all cases, however, the cortical activity has not spread to encompass the occipital pole. Note that this is a different subset of participants than those shown in Fig. 1.

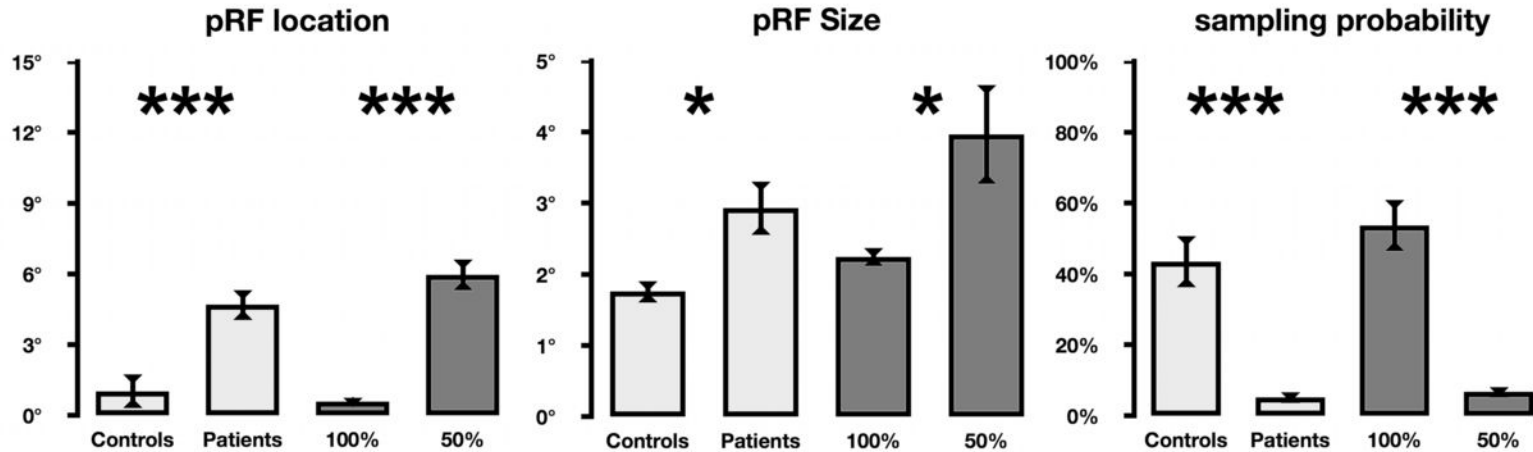
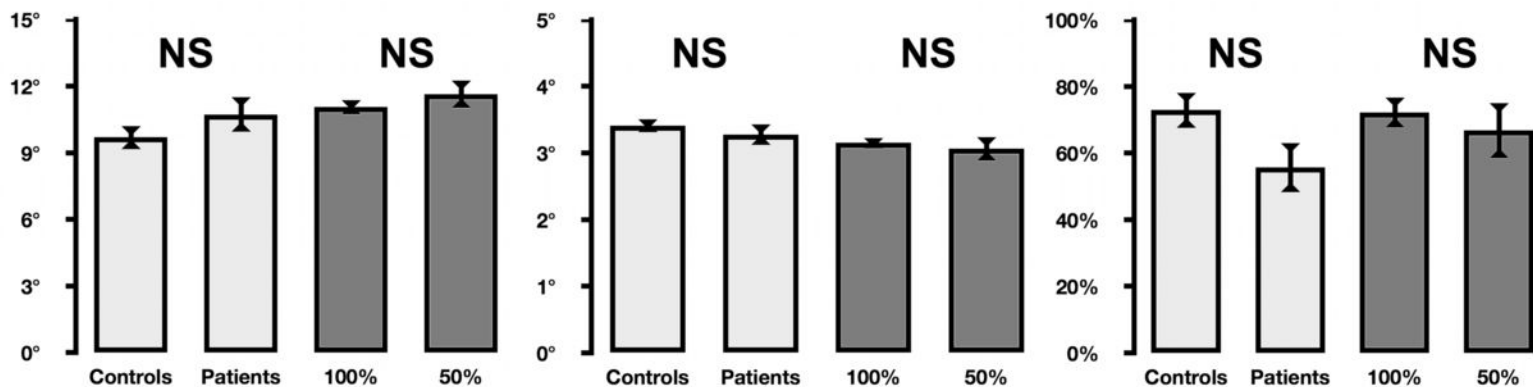
Figure 7: The cortical area representing intact visual field. In panels **a** and **b**, we schematize the method by which the area of primary visual cortex representing a patient's intact visual field (measured by microperimetry) is predicted on the basis of normal retinotopic mapping. First, the primary visual cortex boundary was determined in each control participant by identifying the representations of the of the upper (purple) and lower (green) vertical meridians in calcarine cortex, as indicated by the dotted line on the surface reconstruction of the occipital lobe for one control participant (a). Second, we determine whether a voxel (as indicated by the small square in a and b has a polar angle phase, θ , that is among the values of polar angle in the intact visual field, Θ (see inset false color map showing the location of the scotoma (shaded) and intact (unshaded) regions). If this is the case, as it is in the illustrated example, we then determine whether the eccentricity represented by the voxel, r , is among the eccentricities in the intact field, R , at the polar angle θ . If the voxel's polar co-ordinate (r, θ) is among the set of co-ordinates (R, Θ) of intact visual field locations, the voxel is retained. The **predicted** cortical area representing the patient's intact visual field, A_p , is then computed from all the retained voxels. For each patient, multiple values of A_p (one for each of the age matched control retinotopic maps) were obtained and then averaged to compute the mean predicted area of activated V1, \bar{A}_p . In each patient the area of active primary visual cortex, A_M , was also **measured**. The ratio of A_M to \bar{A}_p is plotted for the participant groups in **c**. No significant differences between groups or between group values and unity were found. Non-significant differences from unity present in the AMD and Simulated Lesion groups are likely due to the minority of 'ectopically' responding voxels found in Fig. 5, which could not be predicted from normal retinotopic maps.



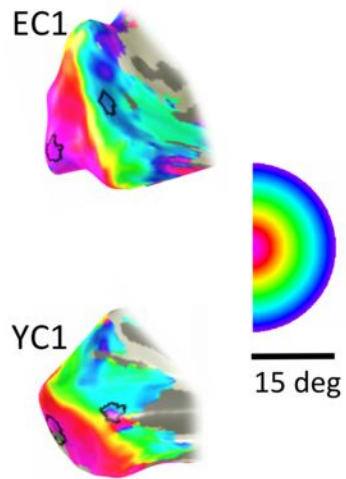






a**b**

a)



b)

